

**THE EFFECTS OF ALKALINE EARTH METALS
IN NiMo-X (X = Mg, Ca, Sr, Ba) CATALYSTS ON
THE CHARACTERISTICS OF CARBON
NANOTUBES DERIVED FROM PLASTICS
PYROLYSIS**

LIM XIU XIAN

UNIVERSITI SAINS MALAYSIA

2024

**THE EFFECTS OF ALKALINE EARTH METALS
IN NiMo-X (X = Mg, Ca, Sr, Ba) CATALYSTS ON
THE CHARACTERISTICS OF CARBON
NANOTUBES DERIVED FROM PLASTICS
PYROLYSIS**

by

LIM XIU XIAN

**Thesis submitted in fulfilment of the requirements
for the degree of
Master of Science**

August 2024

ACKNOWLEDGEMENT

I would like to express my deepest gratitude to Dr. Oh Wen Da for his invaluable guidance, unwavering support, and tireless dedication throughout the duration of this research. Dr. Oh's expertise, insightful feedback, and encouragement have been instrumental in shaping the trajectory of this thesis. Furthermore, I am immensely grateful to Dr. Oh for his pivotal role in securing the necessary funding for this project under Research University Team (RUTeam) Grant Scheme with Project No: 1001/PKIMIA/8580062, without which this research would not have been possible.

I am also indebted to my beloved mother and my dear friend for their spiritual support and encouragement. Their love, understanding, and encouragement have provided me with the strength and motivation to overcome challenges and persevere in the pursuit of academic excellence. Their belief in my abilities has been a constant source of inspiration, and I am truly grateful for their presence throughout this journey.

TABLE OF CONTENTS

ACKNOWLEDGEMENT	ii
TABLE OF CONTENTS	iii
LIST OF TABLES	vi
LIST OF FIGURES	vii
LIST OF SYMBOLS, ABBREVIATIONS AND NOMENCLATURES	xi
LIST OF APPENDICES	xiii
ABSTRAK	xv
ABSTRACT	xvii
CHAPTER 1 INTRODUCTION	1
1.1 Background	1
1.2 Knowledge Gaps and Research Motivation	6
1.3 Objectives and Scope of Study.....	7
1.4 Organization of Thesis	8
CHAPTER 2 LITERATURE REVIEW	11
2.1 Fundamentals of CNTs Synthesis	11
2.1.1 Growth of Different Carbon Products.....	11
2.1.2 Growth Mechanisms of CNTs	12
2.1.3 Factors Affecting the Morphologies of Different Carbon Products ..	19
2.2 Types of Catalysts Applied during CNT Synthesis	21
2.2.1 Alkali Metallic Compounds-Based Catalysts	21
2.2.2 Ni-Based Catalysts	24
2.2.3 Fe-Based Catalysts	34
2.2.4 Co-Based Catalysts	45
2.2.5 Comparison between Ni, Fe, and Co-Based Catalysts.....	52
2.3 Types of Catalyst Supports Applied during CNTs Synthesis	55

2.3.1	Alkali Metallic Compounds-Based Catalyst Supports.....	55
2.3.2	Alkali Earth Metallic Compounds-Based Catalysts Supports	58
2.3.3	Comparison between Catalyst Supports	66
2.4	Summary of Literature Review	69
CHAPTER 3 MATERIALS AND METHODOLOGY.....		70
3.1	Materials.....	70
3.2	Research Methodology.....	70
3.2.1	Synthesis of NiMo-X	70
3.2.2	Characterization of NiMo-X	72
3.2.3	Synthesis of CNTs	74
3.2.4	Characterization of CNTs	75
3.2.5	Characterization of face mask.....	77
3.2.6	Performance studies	78
3.3	Experiment Outline	80
CHAPTER 4 ROLE OF Ca IN NiMo-X CATALYST ON CARBON NANOTUBES GROWTH.....		81
4.1	Introduction	81
4.2	Result and Discussion	82
4.2.1	Sample Characterization	82
4.2.2	One pot synthesis of CNTs using NiMo-Ca-n catalysts	89
4.2.3	Mechanism of CNTs growth.....	99
4.3	Conclusion.....	106
CHAPTER 5 IMPACT OF Ni AND ALKALINE EARTH METAL INTERACTION ON CARBON NANOTUBES PRODUCTION		108
5.1	Introduction	108
5.2	Result and Discussion	109
5.2.1	Characteristics of NiMo-X.....	109

5.2.2	Performance study of NiMo-X.....	116
5.2.3	Characterization of CNTs	122
5.2.4	Optimization study of NiMo-X.....	127
5.2.5	Mechanisms of CNTs synthesis.....	132
5.3	Conclusion.....	135
CHAPTER 6 CONCLUSION AND RECOMMENDATIONS.....		137
6.1	Conclusion.....	137
6.2	Recommendations for future study	139
6.2.1	The quantitative study of CNTs growth and termination mechanisms	139
6.2.2	Catalyst design for CNTs synthesis	140
6.2.3	Environmental impacts study for CNTs synthesis.....	142
6.2.4	CNTs synthesis process design.....	143
REFERENCES		144
APPENDICES		
LIST OF PUBLICATIONS		

LIST OF TABLES

	Page
Table 2.1	Summary of Research on Alkali Metallic Compound-Based Catalysts for CNTs Synthesis. 23
Table 2.2	Summary of Research Involving Ni Catalysts during CNTs Synthesis. 25
Table 2.3	Comparison of the performances of different Ni-based catalysts using CH ₄ as the main carbon source..... 32
Table 2.4	Summary of research involving Fe catalysts during CNTs synthesis. 36
Table 2.5	Comparison of the performances of different Fe-based catalysts using CH ₄ as the main carbon source..... 43
Table 2.6	Summary of research involving Co catalysts during CNTs synthesis. 46
Table 2.7	Comparison of the performances of different Co-based catalysts using CH ₄ as the main carbon source..... 51
Table 2.8	Comparison of the performances among Ni-, Fe-, and Co-based catalysts. All are based on the same operating conditions (CH ₄ carbon source, 700°C OT, 60 min operating duration)..... 54
Table 2.9	Summary of Comparison between Ni-, Fe-, and Co-based Catalysts. 55
Table 2.10	Research involving alkali metallic compound-supported catalysts during CNTs synthesis. 57
Table 2.11	Research involving alkali earth metallic compounds as catalyst supports during CNTs synthesis. 59

LIST OF FIGURES

		Page
Figure 1.1	Schematic illustration of CNTs chirality (a) Representation of metallic or semi-metallic state of CNTs based on the chiral index [7]. (b) Theoretical depiction of CNTs formation [8]. (Appendix A)	2
Figure 1.2	Schematic illustrations of different CNTs synthesis methods. (a) Arc discharge method [10]. (b) Laser ablation method [12]. (c) CVD method [14]. (d) Flame synthesis method [17]. (e) Electrolysis method [19]. (Appendix B)	5
Figure 2.1	Schematic illustrations of different types of carbon nanofibers. The term ‘CNFs’ used in the whole context refers to either platelets CNFs or fishbone CNFs [33]. (Appendix C)	12
Figure 2.2	Schematic illustrations of CNT growth phases and termination phases. (a) Illustration of tip and base growth modes of CNTs. (b) Illustration of tangential and perpendicular growth modes of CNTs. (c) Illustration of the termination phase of CNTs due to catalyst migration factors, covering Ostwald ripening, bulk diffusion of catalyst into the substrate, and consumption of catalyst into CNTs.	16
Figure 2.3	Schematic illustrations of terminated CNT forests. (a) Uniform forest. (b) Delaminated forest. (c) Cracked forest [54]. (Appendix D)	17
Figure 2.4	Schematic illustration of overall growth mechanisms of CNTs.	18
Figure 2.5	Schematic illustrations of CNTs generated from alkali metal catalysts. (a) High tortuosity structure of CNTs produced by NaCl and Na ₂ CO ₃ catalysts [75]. (b) The mechanisms of CNTs formation via sodium chloride catalysts on silicon nitride support [76]. (Appendix E)	24

Figure 2.6	Schematic illustrations of W and Ce promoters to Ni catalysts. (a) Utilization of silica-supported W-Ni catalyst to synthesize SWCNTs with narrow diameters [89] (b) Illustration of the atom trapping characteristic advantage of CeO ₂ as Ni catalysts promoter. (Appendix F).....	31
Figure 2.7	Schematic illustrations of Fe catalyst precursors in synthesizing CNTs. (i) The reaction scheme for FeCl ₂ catalyst in the dehydrogenation reaction of the acetylene carbon source [174]. (ii) The FePO ₄ catalyst synthesized via H ₃ PO ₄ [172]. (Appendix G).....	42
Figure 2.8	Summary of the quantitative performances of Ni-, Fe-, and Co-based catalysts. (a) Carbon yield (%) of Ni-, Fe-, and Co-based catalysts. (b) Diameter (nm) of CNTs generated from Ni-, Fe-, and Co-based catalysts. (c) Porosity (%) of CNTs generated from Ni-, Fe-, and Co-based catalysts. (d) Growth rate (nm/min) of CNTs from Ni-, Fe-, and Co-based catalysts.....	53
Figure 2.9	Schematic illustrations of magnesium compounds as catalyst supports. (a) The optimal orientation for magnesium aluminate crystals was found to be (111), coupled with ion beam bombardment to enhance the yield of CNTs formation [246]. (b) Proposed mechanism for CNTs formation on surfaces with high basicity [253]. (Appendix H).....	64
Figure 2.10	Schematic illustrations of CNTs formation on the surface of CaCO ₃ catalyst support. (a) The triple junction area on the CaCO ₃ -supported catalyst where both surface diffusion and bulk diffusion of carbons occur simultaneously [250]. (b) The cyclic reactions in the triple junction area on the CaCO ₃ catalyst support ensure maximum C ₂ H ₂ conversion for the growth of CNTs. (Appendix I) ..	65
Figure 3.1	Schematic representation of the NiMo-Ca-n catalysts synthesis.	71
Figure 3.2	Schematic representation of the one pot synthesis of CNTs from face masks.	74
Figure 3.3	Outline of the studies.	80

Figure 4.1	(a) FESEM micrograph, and (b-e) elemental mapping of the NiMo-Ca-7.....	87
Figure 4.2	(a) XRD patterns of the NiMo-Ca-n. (b) N ₂ adsorption-desorption isotherms of the NiMo-Ca-n. (c) FTIR spectra of the NiMo-Ca-n. ...	88
Figure 4.3	The carbon yield of the NiMo-Ca-n catalysts under various conditions: (a) Carbon yield with a catalyst to face mask ratio of 3:97 and pyrolysis at 600 °C for 10 min. (b) Carbon yield at different face mask to catalyst ratios. (c) Carbon yield at different pyrolysis temperatures (500 °C, 600 °C, 700 °C) for 10 min. (d) Carbon yield with pyrolysis at 600 °C for different periods (5 to 20 min). (e) Carbon yield after 5 cycles of pyrolysis. (All the FESEM images of the CNTs generated are displayed in Section 4 of the supporting document.).....	94
Figure 4.4	FESEM micrographs of CNTs synthesized using the (a-c) NiMo-Ca-0 (d-f) NiMo-Ca-7 (g-i) NiMo-Ca-15 (j-l) NiMo-Ca-32 and the Gaussian fitting of the outer diameters' distribution of the CNTs produced (m-n) HRTEM images of the CNTs synthesized using the NiMo-Ca-15.	97
Figure 4.5	(a) Raman spectra, and (b) TGA profile of the purified CNTs products.	99
Figure 4.6	The overall CNTs growth mechanisms on NiMo-Ca-n catalysts. ...	100
Figure 5.1	XRD patterns of NiMo-X.....	112
Figure 5.2	FESEM image and elemental mappings of (a) NiMo-Mg, (b) NiMo-MgCa, (c) NiMo-Ca, (d) NiMo-CaSr, (e) NiMo-Sr, and (f) NiMo-Ba	114
Figure 5.3	(a) FTIR spectra, and (b) N ₂ adsorption-desorption isotherms of NiMo-X.....	116
Figure 5.4	The performances of NiMo-X in catalytic pyrolysis of face mask from the perspectives of (a) carbon yield, and (b) gas composition weight fraction analyses. (c) The relative differences of each gas	

	between pre-stream and post-stream of the NiMo-X are calculated.	120
Figure 5.5	The schematic diagram illustrates the impact of X on the performance of NiMo-X in CNTs synthesis, considering both catalyst structure and derivative gases perspectives. "RWGS" in the figure denotes the reverse water gas shift reaction, while "CM" denotes the CO ₂ methanation reaction.	121
Figure 5.6	FESEM images of carbon nanomaterials produced using the (a-c) NiMo-Mg (d-f) NiMo-MgCa (g-i) NiMo-Ca (j-l) NiMo-CaSr (m-o) NiMo-Sr (p-r) NiMoBa and the Gaussian fitting of the outer diameters' distribution of the CNTs produced.....	124
Figure 5.7	(a) Raman spectra, and (b) thermogravimetric analysis (TGA) profile of the purified CNTs products.....	127
Figure 5.8	The optimization of catalytic pyrolysis of face masks via NiMo-X involves manipulating variables such as (a) catalyst to face mask weight ratio (3:97, 1:10, 1:5, 1:3), (b) pyrolysis temperature (500°C, 600°C, 700°C), and (c) pyrolysis duration (5 min, 10 min, 15 min, 20 min). The standard conditions for catalytic pyrolysis of face masks via NiMo-X are 600°C, 10 min, 3:97 catalyst to face mask weight ratio, for 1 cycle. (d) The same NiMo-X was used for continuous pyrolysis with 1.62 g of plastic topped up in each cycle to examine accumulated carbon.	131
Figure 5.9	The schematic diagram illustrates the impact of operating conditions including catalyst to face mask weight ratio, pyrolysis temperature, pyrolysis duration, and pyrolysis cycle, on the performance of NiMo-X in CNTs synthesis.	132

LIST OF SYMBOLS, ABBREVIATIONS AND NOMENCLATURES

CNFs	Carbon Nanofibers
CNTs	Carbon Nanotubes
CQDs	Carbon Quantum Dots
CVD	Chemical Vapor Deposition
DI water	Deionized water
FESEM	Field Emission Scanning Electron Microscopy
FTIR	Fourier Transform Infrared Spectroscopy
GC-TCD	Gas Chromatography-Thermal Conductivity Detector
HRTEM	High Resolution Transmission Electron Microscopy
HDPE	High Density Polyethylene
LDPE	Low Density Polyethylene
LDH	Layered Double Hydroxides
LCA	Life Cycle Analysis
MWCNTs	Multi Walled Carbon Nanotubes
OT	Operating Temperature
PPE	Personal Protective Equipment
PVP	Polyvinylpyrrolidone
PP	Polypropylene
PE	Polyethylene
PS	Polystyrene
PVC	Polyvinylchloride
SWCNTs	Single Walled Carbon Nanotubes
TGA	Thermogravimetric Analysis

X	Alkaline Earth Metals
XRD	X-Ray Diffraction Pattern
VLS	Vapor-Liquid-Solid
VSS	Vapor-Solid-Solid

LIST OF APPENDICES

Appendix A	Permission to reuse figures in Figure 1.1
Appendix B	Permission to reuse figures in Figure 1.2
Appendix C	Permission to reuse figures in Figure 2.1
Appendix D	Permission to reuse figures in Figure 2.3
Appendix E	Permission to reuse figures in Figure 2.5
Appendix F	Permission to reuse figures in Figure 2.6
Appendix G	Permission to reuse figures in Figure 2.7
Appendix H	Permission to reuse figures in Figure 2.9
Appendix I	Permission to reuse figures in Figure 2.10
Appendix J	The mass of different metallic salts used in NiMo-Ca-n and NiMoX synthesis
Appendix K	The characterization of face mask
Appendix L	X-ray Rietveld refinement
Appendix M	Weight fraction of different phases in NiMo-Ca-n and NiMo-X
Appendix N	Average crystallite sizes of different phases in NiMo-Ca-n and NiMo-X catalysts
Appendix O	Average crystallite lattice strain of different phases in NiMo-X
Appendix P	Ni atomic site occupancy in NiO phase presented in each NiMo-X quantification through XRD refinement analysis.
Appendix Q	EDX analysis on NiMo-X
Appendix R	BET and BJH analysis of NiMo-Ca-n and NiMo-X catalysts and sample carbon yield calculation for NiMoCa-15.

- Appendix S The FESEM images of the CNTs synthesized under various operational parameters via NiMo-Ca-15
- Appendix T The XRD profile of the CNTs synthesized via NiMo-Ca-0 and NiMo-Ca-15 catalysts prior to the acid purification
- Appendix U The composition of face mask derived pyrolysis gas and product gas after catalytic pyrolysis via NiMo-Ca-15

**KESAN LOGAM BUMI ALKALI DALAM PEMANGKIN NiMo-X (X = Mg,
Ca, Sr, Ba) TERHADAP CIRI-CIRI NANOTUB KARBON YANG
DIHASILKAN DARIPADA PIROLISIS PLASTIK**

ABSTRAK

Penggunaan pelitup muka yang semakin meningkat telah menimbulkan kebimbangan alam sekitar, yang memerlukan strategi pengurusan sisa yang berkesan. Satu pendekatan yang berkesan adalah dengan mengitar semula sisa plastik pelitup muka menjadi CNTs melalui pirolisis pemangkin. Biasanya, hidrokarbon terhasil daripada plastik pada suhu tinggi, mengkarbonkan pemangkin logam dan membentuk CNTs. Namun, kebanyakan penyelidikan hanya melaporkan penggunaan logam bumi alkali sebagai bahan sokongan termal tanpa menjelaskan kesan mereka terhadap aktiviti pemangkin logam dalam pembentukan CNTs, telah menyekat manipulasi ciri-ciri CNTs untuk aplikasi. Oleh itu, kajian ini bertujuan untuk mengkaji kesan logam bumi alkali terhadap proses pembentukan CNTs daripada perspektif aktiviti permukaan Ni, ciri-ciri permukaan, dan pemuatan fasa logam. Kajian ini menggunakan pemangkin NiMo-Ca-n ($n = 0, 7, 15, \text{ dan } 32$) dan NiMo-X ($X = \text{Mg, Ca, Sr, Ba}$) yang disediakan melalui pembakaran larutan untuk proses pembentukan CNTs daripada pelitup muka. Pada bahagian pertama kajian, didapati bahawa pada pemuatan Ca optimum ($n = 15$), kehadiran fasa CaMoO_4 (14.1 wt.%) dan CaCO_3 (13.4 wt.%) menghasilkan CNTs yang lebih panjang dengan hasil karbon 6.4 wt.% berbanding dengan nanosfera karbon dan serpihan karbon. Peningkatan pemuatan Ca dengan pemuatan fasa CaCO_3 yang tinggi (29.7 wt.%) akan menurunkan hasil karbon ke 5.4 wt.% dengan penampilan CNTs yang pendek. Pada bahagian kedua kajian, didapati bahawa interaksi Ni-X dilemahkan apabila menurun X dalam NiMo-X, telah menjejaskan pembentukan CNTs dan menghasilkan serpihan karbon,

terutamanya daripada NiMo-Ba dengan hasil karbon pada 3.1 wt.%. Kajian menunjukkan bahawa NiMo-Ca dengan interaksi Ni-X yang sederhana, bersama pemuatan permukaan Ni yang sederhana (72.8 at.%), strain fasa NiO yang tinggi (0.00448), dan luas permukaan spesifik yang tinggi ($32.8 \text{ m}^2 \text{ g}^{-1}$), telah menggalakkan pembentukan CNTs yang panjang dengan hasil karbon yang tinggi (6.4 wt.%) kerana kadar metanasi CO_2 yang cepat (204% peningkatan relatif CH_4), kadar nukleasi karbon yang sederhana, dan rintangan penggumpalan Ni yang tinggi. Kajian optimisasi telah menunjukkan bahawa 600°C dan 10 minit adalah keadaan operasi yang optimum, manakala nisbah berat pemangkin kepada pelitup muka yang lebih tinggi dan kitaran pirolisis berterusan dapat meningkatkan hasil karbon hingga 34 wt.% dan $11 \text{ g-C g-cat}^{-1}$. Secara ringkas, kajian ini menyediakan panduan untuk reka bentuk pemangkin dalam proses pembentukan CNTs dengan mengambil kira kefungisian fasa logam, ciri-ciri permukaan pemangkin, dan interaksi terhadap aktiviti Ni.

THE EFFECTS OF ALKALINE EARTH METALS IN NiMo-X (X = Mg, Ca, Sr, Ba) CATALYSTS ON THE CHARACTERISTICS OF CARBON NANOTUBES DERIVED FROM PLASTICS PYROLYSIS

ABSTRACT

The increased usage of face masks has spurred environmental concerns, necessitating effective waste management strategies. One effective approach is to upcycle face mask plastic waste into carbon nanotubes (CNTs) through catalytic pyrolysis. Typically, the plastic-derived hydrocarbons, at high temperatures, contact the metal catalysts, allowing the supersaturation state of metal carbide and the formation of CNTs. To date, most research only reports the alkali earth metal elements as thermal supporting material without clarifying their impacts on metal activity in CNTs synthesis, limiting the manipulation of CNTs characteristic for applications. As such, this study aims to investigate the impacts of alkali earth metals towards the CNTs synthesis from the perspective of surface Ni activity, surface characteristic, and metal phases loading. This study utilized the NiMo-Ca-n (n = 0, 7, 15, and 32) and NiMo-X (X = Mg, Ca, Sr, Ba) catalysts prepared via solution combustion synthesis for one-pot synthesis of CNTs from face masks. In the first part of the study, it was discovered that at optimum Ca loading (n = 15), the presence of CaMoO₄ (14.1 wt.%) and CaCO₃ (13.4 wt.%) phases yielded longer CNTs with a carbon yield of 6.4 wt.% instead of carbon nanospheres and carbon fragments. Further increase in Ca loading with a high CaCO₃ fraction (29.7 wt.%) would lower its carbon yield to 5.4 wt.% with short CNTs appearance. In the second part of the study, it was found that weaker Ni-X interaction moving down the Group 2 elements within NiMo-X jeopardizes the formation of CNTs, resulting in carbon flakes instead, especially from NiMo-Ba with a carbon yield at 3.1 wt.%. It was shown that NiMo-Ca with moderate Ni-X interaction, a moderate

surface Ni fraction (72.8 at.%), high NiO lattice strain (0.00448), and high specific surface area ($32.8 \text{ m}^2 \text{ g}^{-1}$), promoted long CNTs with high carbon yield (6.4 wt.%) due to a high CO_2 methanation rate (204% relative increment of CH_4), moderate carbon nucleation rate, and high sintering deactivation resistance. The optimization studies had shown that 600°C and 10 min were the optimum operating conditions, while a higher catalyst to face mask weight ratio and continuous pyrolysis cycles may further enhance its carbon yield up to 34 wt.% and $11 \text{ g-C g-cat}^{-1}$. In short, this study provides guidance on catalyst design for CNTs synthesis in consideration of functionalities of metal phases, surface characteristic of catalyst, and the compartment interaction towards the Ni activity.

CHAPTER 1

INTRODUCTION

1.1 Background

Since the onset of the COVID-19 pandemic, there has been a significant surge in the usage of Personal Protective Equipment (PPE) such as medical face masks, gloves, and test kits. This heightened demand has led to a concerning increase in the accumulation of plastic waste globally. Consequently, there has been a growing awareness about the environmental hazards associated with the improper disposal of these PPE items, prompting efforts to highlight the importance of plastic recycling and upcycling. Statistics reveal the alarming scale of the issue. In India alone, the volume of medical waste surged from 3025 tons in June 2021 to 4253 tons in July 2021, and further to 5238 tons in August 2021 [1]. Similarly, countries like Brazil and South America are grappling with significant plastic waste generation, with staggering figures such as 85 million and 380 million face mask wastes generated per day, respectively [2,3]. According to MIT News, the global population has generated an estimated 7200 tons of medical waste, primarily from the disposal of medical face masks. These figures underscore the urgent need to address this issue by promoting the upcycling and recycling of plastic waste. By adopting sustainable practices and innovative solutions, we can mitigate the environmental impact of PPE waste while simultaneously creating valuable resources from discarded materials.

In many countries, the predominant methods for managing plastic waste involve incineration and landfilling, both of which pose significant environmental risks, including greenhouse gas emissions and pollution of air, soil, and water. To address these challenges, research efforts have increasingly focused on the catalytic

conversion of plastic waste into valuable resources such as oil fuels, syngas, and carbon nanomaterials. Among these carbon nanoproducts, carbon nanotubes (CNTs) have emerged as a promising solution. CNTs represent an allotrope of pure carbon characterized by a cylindrical hexagonal lattice structure. Renowned for their exceptional properties, they exhibit high thermal conductivity [4], electrical conductivity [5], and tensile strength. However, these attributes are closely tied to the predetermined chiral index (n,m) . Specifically, CNTs can exist in a metallic state when $n - m = 0 \pmod{3}$ or a semi-metallic state when $n - m = 1$ or $2 \pmod{3}$ (as depicted in **Figure 1.1a**) [6,7]. **Figure 1.1b** illustrates the theoretical formation of CNTs by rotating them in the direction of the predetermined chiral vector, \vec{C} where $\vec{C} = n\vec{a} + m\vec{b}$, \vec{a} and \vec{b} are the hexagonal lattice unit vectors, and n and m represent the magnitudes of the respective lattice unit vectors [8].

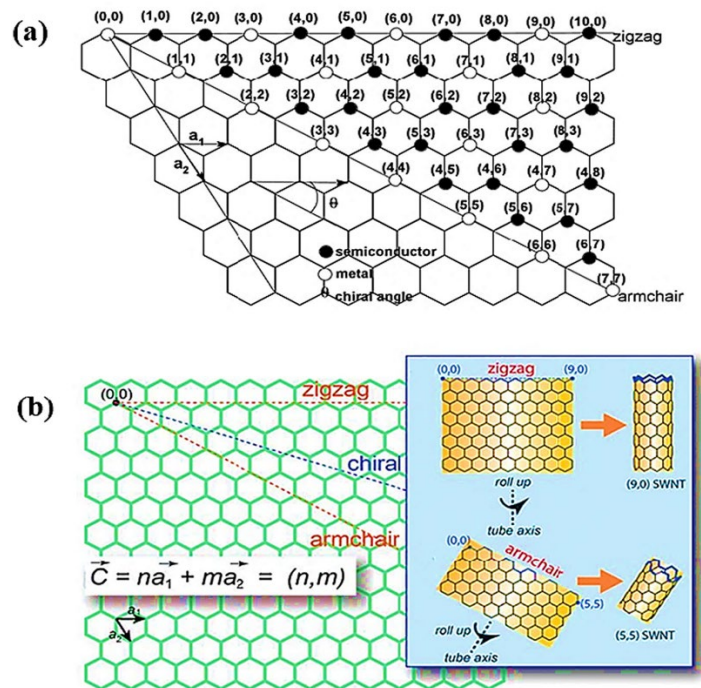


Figure 1.1 Schematic illustration of CNTs chirality (a) Representation of metallic or semi-metallic state of CNTs based on the chiral index [7]. (b) Theoretical depiction of CNTs formation [8]. (References permission: Appendix A)

Several methods exist for generating CNTs, including the arc discharge method [9,10], laser ablation method [11,12], chemical vapor deposition (CVD) methods [13,14], mechano-thermal synthesis method [15], flame synthesis method [16,17], and electrolysis method [18,19]. The arc discharge method involves passing direct current arc voltage through two graphite electrodes under an inert gas environment (as depicted in **Figure 1.2a**) [9]. The resulting CNTs can be collected at the graphite cathode. Typically, multi walled carbon nanotubes (MWCNTs) are obtained using a pure graphite anode, while single walled carbon nanotubes (SWCNTs) are obtained using a metal-doped graphite anode via the arc discharge method. In the laser ablation method, a pulsed laser system is utilized to target graphite samples in a high-temperature reactor for CNTs generation (**Figure 1.2b**). The formed CNTs are then transferred to a cooled collector with the aid of inert gases at high pressure [11]. Meanwhile, CVD synthesizes CNTs by continuously flowing hydrocarbon gases through a catalyst at high temperature (**Figure 1.2c**) [20]. Instead of using laser approaches to decompose graphite sources, some researchers have explored the mechano-thermal synthesis method as an alternative. This involves milling graphite flakes prior to thermal annealing of the graphite nanopowder into CNTs at high temperature [15]. Additionally, the flame synthesis method proposes a direct application of a premixed flame, consisting of fuels and oxidizing agent, onto catalysts for CNTs production (**Figure 1.2d**) [16]. Finally, similar to the arc discharge method, the electrolysis method operates with graphite electrodes immersed in solutions to synthesize CNTs (**Figure 1.2e**) [18].

Among the various types of CNTs synthesis methods, the CVD method has garnered popularity in research circles due to its process flexibility. For instance, methods such as arc discharge, laser ablation, mechano-thermal, and electrolysis solely

utilize raw graphite materials for CNTs generation. This limitation restricts their flexibility in employing different carbon precursors and scalability, as they require substantial graphite sources to produce CNTs. Recent studies suggest the feasibility of producing CNTs from pyrolytic gas derived from plastics using the CVD method. This highlights the flexibility of the CVD process and opens opportunities for industrial-scale production. Furthermore, the flame synthesis method often exhibits inferior performance compared to the CVD method, primarily due to the significant formation of soot nanoparticles. This phenomenon is attributed to the potential formation of $\cdot\text{OH}$ radicals, which induce an etching effect on CNTs through continuous O_2 supply. Additionally, the unstable conditions of reactors, caused by the uneven temperature profile of substrates produced by flames, contribute to this outcome.

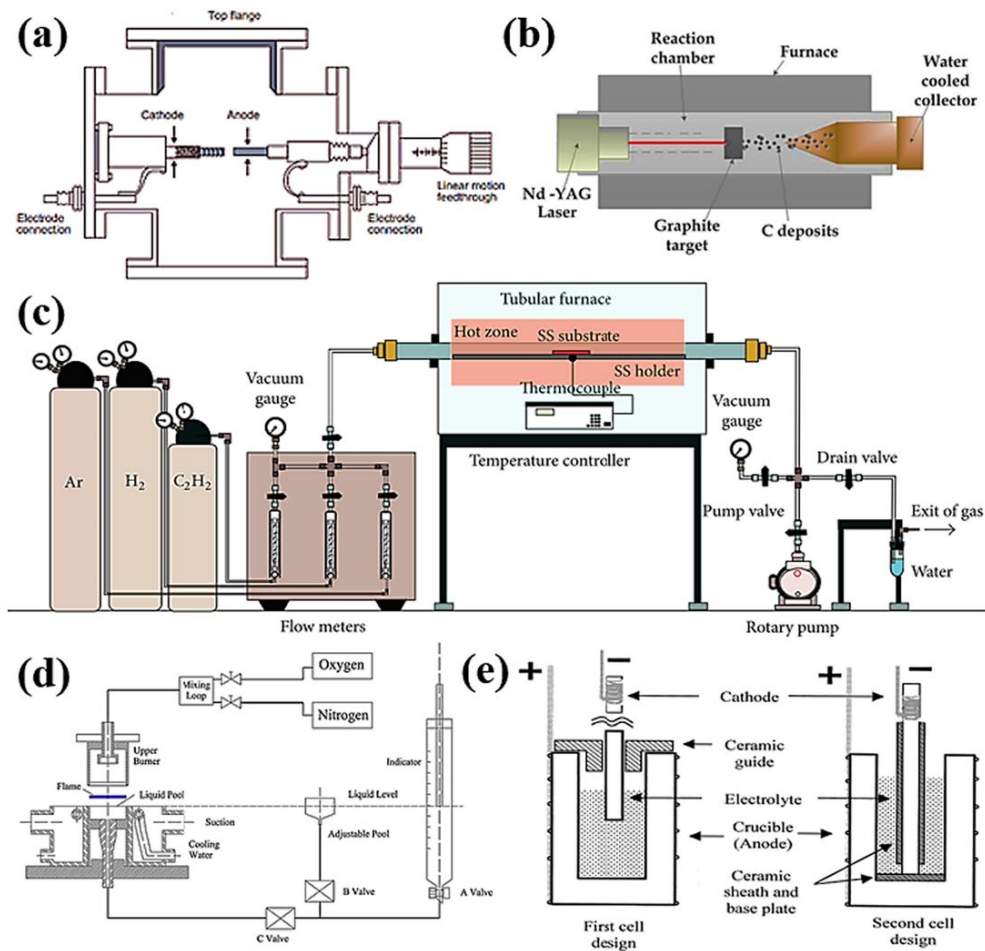


Figure 1.2 Schematic illustrations of different CNTs synthesis methods. (a) Arc discharge method [10]. (b) Laser ablation method [12]. (c) CVD method [14]. (d) Flame synthesis method [17]. (e) Electrolysis method [19]. **(References permission: Appendix B)**

The CVD method has been predominantly utilized for the synthesis of CNTs from plastic waste. Numerous studies have explored various aspects of catalytic conversion, including process flow schemes, types of plastic feedstocks, catalyst designs, optimization of operating variables, and potential real-world applications of CNTs. These investigations play a crucial role in advancing our understanding of this innovative approach to plastic waste management and its broader implications for environmental sustainability. Moreover, they contribute to promoting potential applications of CNTs across diverse fields, including electronics, energy storage, membrane separations, strengthening filler composites, and catalysis.

1.2 Knowledge Gaps and Research Motivation

In conventional CVD procedures for producing CNTs, a typical setup involves a pyrolysis reactor for plastic cracking and a CVD reactor for carbon deposition, connected to an inert N₂ gas source. Simultaneously, recent research has also explored more streamlined synthesis approaches, such as one-pot methods like catalytic flame synthesis, muffle furnace pyrolysis, and microwave irradiation synthesis methods. Generally, the metal catalysts used can be classified into three main groups: main metal catalysts for CNTs growth, promoters, and thermal stability supports. Among the main metal catalysts for CNTs growth, Ni-based catalysts are more frequently employed compared to Fe-based and Co-based catalysts for CNTs growth due to their higher CNTs growth rate [21]. Additionally, Fe-based and Co-based catalysts tend to produce CNFs and amorphous carbon flakes, which are less favorable. For promoters, Mo-based promoters are preferred due to their ability to store carbon through the formation of molybdenum carbide, subsequently aiding CNTs growth by supplying carbon to the adjacent metal catalyst[22]. For thermal stability supports, alkaline earth metal elements such as Mg, Ca, Sr, and Ba are favored due to their high surface basicity, which eases the acid purification process of carbon products to obtain CNTs.

To date, there has been limited research dedicated to exploring the roles of supports, especially alkaline earth metal elements, in CNT growth, with unclear catalytic mechanisms. For example, some studies have reported on the performance of NiMo/MgO catalysts for CNT synthesis with varying Ni, Mo, and Mg loadings [23], but they lack analysis on the impact of support loading on the produced CNTs, such as the morphologies of total carbon products and their characteristics. Secondly, other studies have highlighted the superior performance of Ni/La and Ni/Sr catalysts over Ni/Mg catalysts without thorough reasoning on the impacts of Ni-support interactions

on CNT growth [24]. Thirdly, there is a gap in understanding the effects of distinct catalyst phases and Ni-X interactions on the quantity of pyrolytic gases and the generated carbon products. Lastly, there is a need to understand the impacts of various operating parameters through optimization. While some past studies have focused on enhancing catalyst activity by incorporating alkaline earth metals for CNT production via traditional CVD methods, most have only examined the diameter characteristics of CNTs concerning metal-support interactions and sintering degradation resistance [25]. Therefore, the aforementioned four main research gaps require identification and investigation.

1.3 Objectives and Scope of Study

This study aims to address these gaps by pursuing the following objectives:

1. Evaluating the impacts of various Ca loading in NiMo-Ca-n catalysts towards the morphologies and characteristics of synthesized CNTs through phase study.
2. Investigating the contributions of Ni-X interaction moving down the Group 2 elements in NiMo-X catalysts towards the morphologies and characteristics of synthesized CNTs.
3. Quantifying the yields of pyrolyzed hydrocarbons and carbon to represent the activities of NiMo-Ca-n and NiMo-X catalysts in catalytic cracking of plastic.
4. Optimizing the performance characteristics exhibited by NiMo-Ca-n and NiMo-X catalysts under varying operational conditions, including pyrolysis temperature, pyrolysis duration, catalyst-to-face-mask ratio, and multiple pyrolysis cycles.

By undertaking these objectives, this study contributes to the advancement of knowledge in the field of CNTs synthesis and catalyst design. It enhances our

comprehension of the intricate processes involved in the one-pot conversion of plastics into valuable carbon nanomaterials.

1.4 Organization of Thesis

This thesis comprises six chapters, namely: (i) Introduction, (ii) Literature Review, (iii) Materials and Research Methodology, (iv) Results and Discussion (divided into two chapters), and (v) Conclusions and Recommendations.

Chapter 1: INTRODUCTION

This chapter serves to provide the background knowledge of the catalytic synthesis of CNTs from plastic and discusses the current knowledge gap regarding the one-pot synthesis of CNTs from plastic. Additionally, it outlines the research objectives and the organization of the thesis.

Chapter 2: LITERATURE REVIEW

This chapter provides relevant literature reviews emphasizing catalyst design strategies based on different elements for CNTs synthesis. It begins by discussing the general CNTs growth mechanism, covering nucleation, growth, and termination phases, and introduces factors affecting CNTs growth. The chapter thoroughly explores the characteristics of various types of catalysts, including alkali metal-, Ni-, Fe-, and Co-based catalysts, and compares their performances. Additionally, different types of catalyst supports, such as alkali metal and alkali earth metal catalyst supports, are discussed in detail, including comparisons between them.

Chapter 3: MATERIALS AND METHODOLOGY

This chapter provides a comprehensive overview of the preparation of NiMo-X catalysts, followed by the procedures for the one-pot synthesis of CNTs from plastic. It includes detailed descriptions of the characterization studies and performance evaluations.

Chapter 4: ROLE OF Ca in NiMo-X CATALYST ON CARBON NANOTUBES GROWTH

This chapter describes the preparation of NiMo-Ca catalyst with different Ca loadings, followed by characterization to investigate both intrinsic and extrinsic properties. Subsequently, the carbon yield of NiMo-Ca with various Ca loadings and the characterization of the synthesized CNTs were investigated. Finally, the impact of various Ca loadings in NiMo-Ca on the CNT growth mechanism was presented.

Chapter 5: IMPACT OF Ni AND ALKALINE EARTH METAL INTERACTION IN CARBON NANOTUBES PRODUCTION

This chapter provides an overview of the preparation of NiMo-X catalyst, followed by characterization to examine both intrinsic and extrinsic properties. Subsequently, it delves into the investigation of the carbon yield of NiMo-X and the characterization of the synthesized CNTs. Finally, the chapter discusses the impact of different alkaline earth metal elements in NiMo-X on the morphologies of CNTs and their growth mechanism.

Chapter 6: CONCLUSIONS AND RECOMMENDATIONS

This chapter summarizes both studies from Chapters 4 and 5. Additionally, it outlines four future research directions, covering: (1) statistical modeling of the growth and termination of the CNTs process via quantitative and qualitative measures, (2) optimum catalyst design strategies encompassing types of catalysts, supports, and catalyst precursors, (3) evaluation of the sustainability of CNTs production through life cycle assessments, and (4) development of optimal process flows with high robustness

CHAPTER 2

LITERATURE REVIEW

2.1 Fundamentals of CNTs Synthesis

2.1.1 Growth of Different Carbon Products

Generally, diverse types of carbon products, including carbon nanosheets, carbon nanofibers, and carbon nanospheres, can be generated under different conditions. Carbon nanosheets, also known as graphene, are characterized by a 2D carbon layer structure with a honeycomb lattice formation. When a single 2D layer of graphene is rolled up into a 3D cylinder structure, SWCNTs are produced. However, in most cases, MWCNTs are more commonly obtained, consisting of several layers of graphene stacked together to form a multi-walled tubular carbon structure. Occasionally, both SWCNTs and MWCNTs may be referred to as tubular carbon nanofibers (CNFs). **Figure 2.1** depicts different types of carbon nanofibers, including tubular CNFs, platelets CNFs, and fishbone CNFs. Instead of generating hollow core types of tubular CNFs, platelets CNFs, and fishbone CNFs with almost solid cores may be synthesized. The primary difference among tubular CNFs, platelets CNFs, and fishbone CNFs lies in the angle between the graphene plane and the fiber growth axis. In MWCNTs, the angle of the graphene plane is parallel to the fiber growth axis. In platelets CNFs, the angle of the graphene plane is normal to the fiber growth axis. In fishbone CNFs, the angle is somewhere between that of CNTs and platelets CNFs.

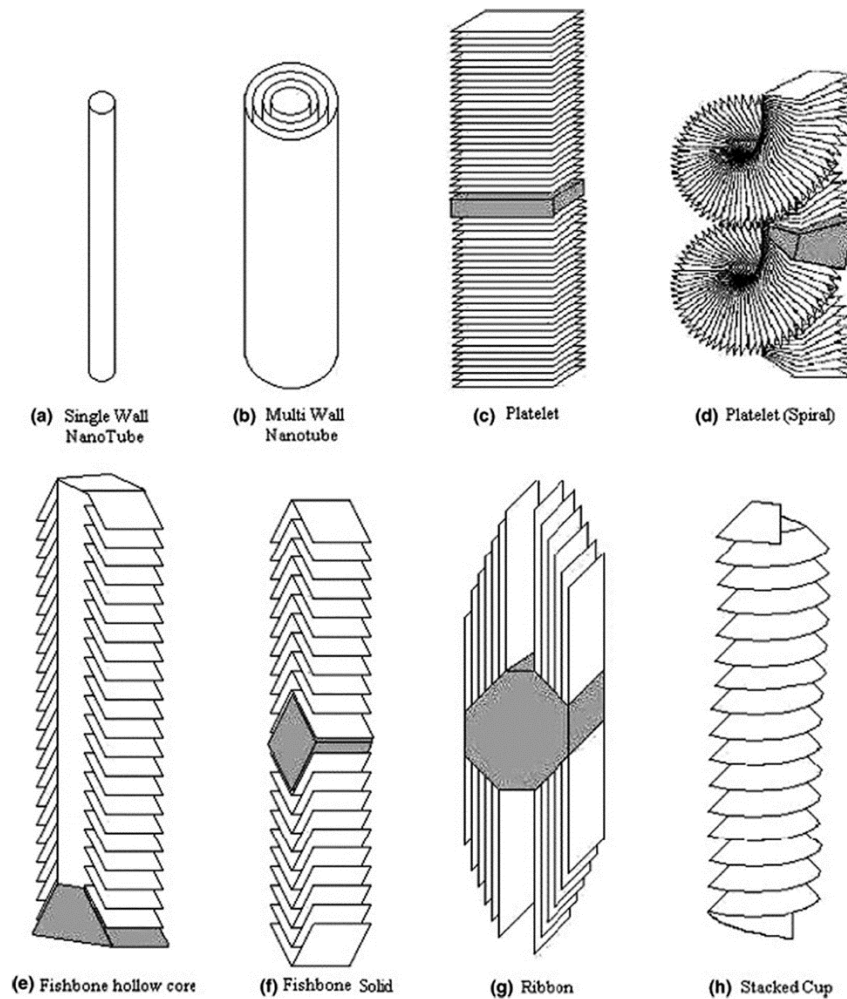


Figure 2.1 Schematic illustrations of different types of carbon nanofibers. The term ‘CNFs’ used in the whole context refers to either platelets CNFs or fishbone CNFs [26]. (References permission: Appendix C)

2.1.2 Growth Mechanisms of CNTs

Since CVD is the most applicable technique in CNTs synthesis, this section discusses the growth mechanisms of CNTs based on the CVD method. It covers continuum-phenomenological growth and atomistic simulation, which encompass nucleation (graphitization), growth, and termination phases. Generally, three types of controversial nucleation models are proposed: bulk diffusion [27], surface diffusion [28], and carbide formation models [29]. In the bulk diffusion model, carbons from the surrounding graphitic layers decompose into carbon atoms and diffuse into the subsurface of the catalyst due to the carbon concentration gradient. Subsequently,

these carbon atoms diffuse out immediately from the catalyst layers and graphitize as hexagonal carbon rings on its surfaces, initiating the growth of CNTs. On the other hand, the surface diffusion model assumes that carbon atoms derived from the surrounding graphitic layers migrate directly from the attachment points to the nucleation site for CNT growth. Usually, the bulk diffusion model and the surface diffusion model are likely to occur on the surface and subsurface of the catalysts, which exist in the solid state; hence they are also frequently cited as the Vapor-Solid-Solid (VSS) mechanism.

The third model for the nucleation of CNTs is the carbide formation model. This model was proposed based on the discovery that CNTs could be successfully developed by solely heating carbon-containing Fe precursors, such as Fe(II) phthalocyanine, without any external carbon sources. During this process, the decomposition of Fe carbide is indeed required, leading to the conclusion of the carbide formation model. The high-energy irradiations decompose the carbon vapors into carbon atoms. These carbon atoms then diffuse into the Fe catalyst, where they form Fe carbide. With the continuous supply of carbon sources over the reaction time, the supersaturation of the carbide loading is achieved. Subsequently, the carbon atoms diffuse out from the Fe carbide matrix and segregate as CNTs. Typically, the carbide formation model is consistent with the Vapor-Liquid-Solid (VLS) model [30], which suggests that catalysts are in a liquid state during the high-temperature synthesis of CNTs. This liquid state facilitates the uptake of carbons and the formation of the carbide phase.

Moreover, the growth phase of CNTs is commonly described by four models: tip growth [31,32], base growth [33,34], tangential growth [35,36], and perpendicular growth models [35,36]. According to the tip growth model [37–39], a fraction of the

catalyst is released from the host catalyst and moves in the direction of CNT growth. Upon termination of CNT growth, the catalyst is either located at the tip of the CNTs or encapsulated within them. On the other hand, the base growth model [34] illustrates CNT growth, with most of the catalysts remaining stationary at the bottom of the CNTs. No catalyst is encapsulated in the inner walls of CNTs after the CVD process (**Figure 2.2a**). Generally, it is believed that both the small size of the catalyst [40] and high operating temperature (OT) conditions [41] lead to base growth mode, and vice versa. In addition, the proposed tangential growth model indicates that the growth of CNTs is tangential to the surface of the catalyst nanoparticles, while the perpendicular growth mode is otherwise (**Figure 2.2b**) [35]. Usually, the perpendicular growth model is observed in the early stage of the CNTs synthesis process due to the high concentration of carbon fraction in the catalyst. After a considerable time, during which the carbon fraction in the catalyst is consumed for CNTs growth, the tangential growth mode is observed [36]. Since a large area of the catalyst is in contact with the graphitic layers during the tangential growth mode, it is unsurprising that the catalyst deactivates rapidly due to carbon coking.

Finally, the termination phase of CNTs is thoroughly discussed based on catalyst migration [31,42,43] and steric hindrance factors. For catalyst migration factors, Ostwald ripening [42], bulk diffusion of the catalyst into the substrate [43], and consumption of the catalyst into CNTs (tip growth mode) [35], are detailed (**Figure 2.2c**). In most cases, the exceptionally high temperature of the CVD process increases the overall kinetic energy of the catalyst and accelerates its migration over the substrate surface. Catalyst nanoparticles with small sizes diffuse and adhere to larger catalyst nanoparticles, resulting in the coalescence of larger catalyst clusters, a phenomenon often called Ostwald ripening. Consequently, Ostwald ripening broadens

the size distribution of the nanoparticles and speeds up the termination phase of CNTs. Catalyst nanoparticles with larger sizes are likely to be underfed by carbon sources, making them unable to initiate the growth of CNTs due to low carbon saturation. Conversely, catalyst nanoparticles with smaller sizes face the issue of carbon loading oversaturation. Thick graphitic layers may detach from the surface of the catalyst due to weak adhesion, allowing nanoparticles to be encapsulated in carbon cages and prohibiting the growth of CNTs [44].

Moreover, it is revealed that catalyst sizes become smaller due to the subsurface diffusion of catalyst into substrate films [43]. To address this issue, it is highly suggested to implement immediate preheating of the catalyst at very high temperatures to densify the substrate. A similar issue is observed for CNTs undergoing tip growth mode, where the catalysts are consumed into the hollow tube of CNTs. To rectify this problem, it is recommended to implement a continuous supply of catalysts through the floating CVD method to compensate for the loss of catalysts in CNTs. Undoubtedly, both the bulk diffusion of catalyst nanoparticles into the substrate and the consumption of catalyst into CNTs scenarios cause the loss of some portion of the catalyst, which ultimately leads to carbon encapsulation followed by termination of the growth of CNTs.

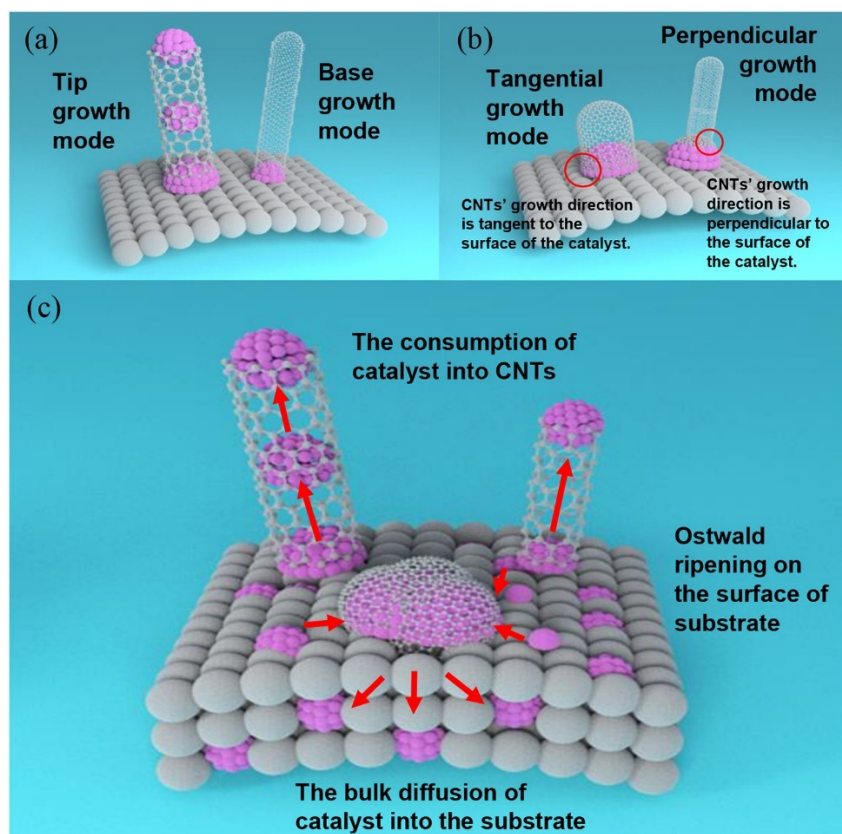


Figure 2.2 Schematic illustrations of CNT growth phases and termination phases. (a) Illustration of tip and base growth modes of CNTs. (b) Illustration of tangential and perpendicular growth modes of CNTs. (c) Illustration of the termination phase of CNTs due to catalyst migration factors, covering Ostwald ripening, bulk diffusion of catalyst into the substrate, and consumption of catalyst into CNTs.

In addition, strain built up due to tube-tube interaction (cohesive energy) and tube-catalyst nanoparticle interaction (adhesive energy) are ascertained to play important roles in the termination phase of CNTs. During the termination phase of vertically aligned CNTs, there is a loss of alignment at the bottom end of CNTs, while the upper parts of CNTs remain aligned. The unaligned CNTs phenomenon is postulated due to the strain built up through both the mechanical drag force exerted by surrounding CNTs in either Van der Waals attractions or repulsions and the adhesive pulling force between CNTs and catalyst [42,45,46]. Generally, the termination of vertically aligned CNTs results in forms such as the uniform forest, delaminated forest, and cracked forest (**Figure 2.3**) [47]. Such morphology differences in terminated CNTs are highly correlated with the height of CNTs, where delaminated and cracked forests dominate

at high and low forest heights, respectively. At low CNT forest heights, the degree of adhesive force between CNT-catalyst is more substantial; hence, the strain is relieved through the reduction of cohesive energy between CNTs, and vice versa. In short, the strain built up terminates the growth of CNTs in various morphologies. To date, the growth mode of CNTs remains controversial among researchers as it is challenging to identify real-time interactions between carbon sources and catalysts. **Figure 2.4** summarizes all the possible growth mechanisms of CNTs from nucleation to termination phase.

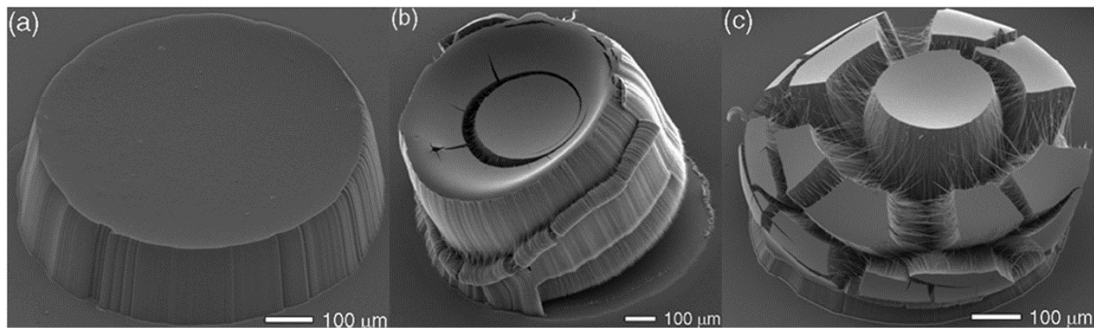


Figure 2.3 Schematic illustrations of terminated CNT forests. (a) Uniform forest. (b) Delaminated forest. (c) Cracked forest [47]. (**References permission: Appendix D**)

CNTs overall growth mechanisms

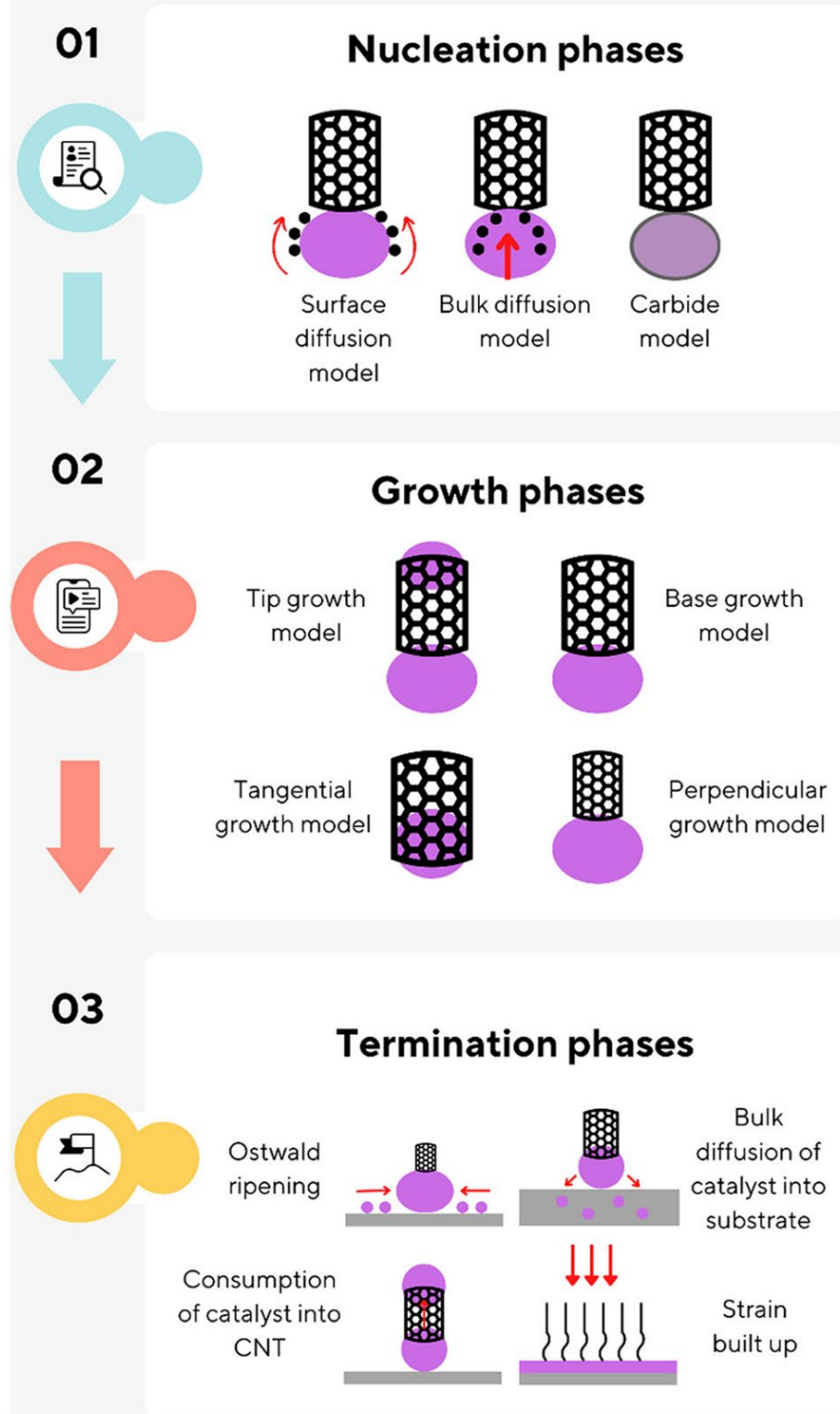


Figure 2.4 Schematic illustration of overall growth mechanisms of CNTs.

To summarize, attention should be given to the selection of catalyst types or the manipulation of metal loading in composite catalysts, focusing on their carbon solubilities and strategies to control the size distributions of catalyst nanoparticles during the synthesis of CNTs. According to the tangential growth model, catalysts with low carbon solubility are undesirable as they lead to faster deactivation via carbon encapsulation. Furthermore, efforts should be made to prevent the broadening of size distributions of catalyst nanoparticles, as discussed in the termination phase of CNTs. For example, the utilization of polyoxometalate catalyst precursors during CNTs synthesis can enhance chirality selectivity growth [48] and may inhibit catalyst nanoparticle sintering [49].

2.1.3 Factors Affecting the Morphologies of Different Carbon Products

Three main factors affecting the morphologies of different carbon products are identified, including the types of catalyst, OT, and composition of feedstock gases. In the following section, the details regarding the nature and stability of various metal catalysts are discussed. High OT generally favor the formation of CNTs over other carbon products [50–53]. By providing sufficient thermal energy, metal catalysts with high surface energy may periodically reshape and undergo contraction/elongation, thus providing more step edges favorable for CNTs growth [54]. Further increases in the OT may result in the formation of bamboo-like CNTs [52] or carbon nanosphere [55]. This phenomenon can be explained from two perspectives: catalyst sintering and the reactivity of the metal catalyst towards carbon feedstock. Severe catalyst sintering produces large catalyst nanoclusters with insufficient surface energy for reshaping, favoring a pear-shaped carbon fiber structure (bamboo-like CNTs) [54]. Additionally, extremely high OTs induce a high catalyst activity towards carbon feedstock and a higher carbon deposition rate than carbon consumption rate, leading to the formation

of carbon nanospheres. Conversely, lower OT favor the growth of CNFs [50,52] or carbon nanosheets [55].

In addition, the composition of the carbon feedstock plays a pivotal role in affecting the characteristics of different carbon products. A comparison of aliphatic, aromatic, and cyclic hydrocarbon sources, such as C₆H₁₄, C₆H₆, and C₆H₁₂, at an optimized OT revealed distinct outcomes. It was previously observed that C₆H₁₄ and C₆H₁₂ carbon sources lead to the formation of MWCNTs and carbon flakes, while C₆H₆ results in the formation of SWCNTs [56–58]. For instance, from thermodynamic perspectives, C₆H₁₄ and C₆H₁₂, which have lower Gibbs free energy than C₆H₆ in the thermal decomposition reaction at 800°C, are more prone to C-C cleavage, thus forming more carbon fragments and MWCNTs instead [56,59]. Although both CH₄ and C₆H₆ hydrocarbon sources showed comparable formation of high-quality SWCNTs, C₆H₆ only initiated CNTs growth at OT > 800°C, with slightly higher CNTs porosity [56,60], while CH₄ can initiate CNTs growth from 600°C and above via catalytic cracking, as shown in **Equation 2.1**.



Additionally, olefin sources, especially C₂H₂, were generally observed to yield more CNTs than CH₄ or any other alkane sources [61,62]. This observation could be attributed to the lower energy requirement for breaking the C-C π bond and the formation of free radicals from its derivatives to attack the C-C bond, providing more carbon supply to the catalysts [63]. Furthermore, the involvement of oxygen-containing hydrocarbons such as CO, CO₂, and C₂H₅OH promotes the oxidation of catalysts, especially Fe-based catalysts, enhancing the formation of H₂ and H₂O for controlled deposition of carbon and growth of MWCNTs [62,64]. In summary, significant factors affecting the morphologies of carbon products, including the types

of catalyst, OT, and composition of feedstock gases, provide guidelines for the optimized growth of specific carbon products. However, other factors such as the presence of impurities in feedstock gases [26] derived from plastic wastes, feedstock gas supply rate [65], and proportion of etcher sources in feedstock gases [66] still require further research, aside from the major factors mentioned, for the sustainable growth of CNTs.

2.2 Types of Catalysts Applied during CNT Synthesis

2.2.1 Alkali Metallic Compounds-Based Catalysts

Table 2.1 presents the performance of alkali metallic compounds such as NaCl, Na₂SO₄, Na₂CO₃, NaHCO₃, Na₂CO₃, NaOH, KCl, K₂SO₄, K₂CO₃, and KI as catalysts for generating CNTs. In general, the carbon products generated from alkali metallic catalysts mainly consist of CNTs with twisted structures and amorphous carbons due to (i) the anisotropic nature of different surface facets possessed by alkali metallic catalysts and (ii) the instability of alkali metallic catalysts under high-temperature CVD processes [67]. Specifically, alkali metallic catalysts with relatively low melting points tend to dissociate and undergo shape fluctuation in the high-temperature CVD process. At the same time, alkali metallic catalysts are incapable of decomposing hydrocarbons, and they solely act as the nucleation site for CNTs growth, leading to the generation of low yield, branched, and twisted CNTs with onion-like tips (**Figure 2.5a**) [68]. The growth mechanism of CNTs via Na catalysts is summarized as follows: Firstly, the carbothermal reduction of Na compounds catalysts occurs (regardless of the counter ions), and the metallic Na acts as the main catalyst for CNT growth. Then, the metallic Na catalysts react with hydrocarbons to form Na carbides and subsequently decompose under an H₂ environment to provide graphitic carbon for CNTs nucleation. Fiber-like structures with an outer core mainly occupied with carbon

elements while the inner core mostly occupied with Na carbonate compounds, grow with time. Finally, the depletion of the Na element in the inner core of CNTs commences from the tips of CNTs to the base and finally results in metal-free CNTs (**Figure 2.5b**).

In general, CNTs with high tortuosity and porous structures are commonly observed during synthesis at high temperatures using alkali metallic catalysts. One of the key advantages of using alkali metallic catalysts for CNTs synthesis is the ease of extracting metal-free CNTs by simple washing or thermal treatment at low temperatures, owing to the high solubility of alkali metals in water and their relatively low melting points. However, a significant challenge in utilizing alkali metallic catalysts for CNTs synthesis is their instability at very high CVD temperatures, which can lead to a loss of catalytic activity in CNTs generation [68,69]. While further research is needed to determine the stability and yield of CNTs produced using alkali metallic compound catalysts, exploring other alkali metallic compounds with higher melting points, such as Na_2SiO_3 , NaAlO_2 , and NaF , may offer more stable production of CNTs.

Table 2.1 Summary of Research on Alkali Metallic Compound-Based Catalysts for CNTs Synthesis.

Catalysts / Metallic precursors / Substrates	Catalysts synthesis method	Carbon sources / Growth conditions	Catalysts performances	Ref
CaCO ₃ supported Fe-Co-K / Co(CH ₃ COO) ₂ , Fe(C ₁₅ H ₂₁ O ₆), and potassium compounds / CaCO ₃	Coprecipitation	Acetylene / CVD at 720°C	<ul style="list-style-type: none"> Carbon yield: 2.6388 wt.% (Co:Fe = 1:1 with 3% K dopants) Porous and bundle-like SWCNTs were synthesized. 	[70]
Potassium iodide / - / -	Raw	Acetylene / CVD at 500-700°C for 60 min	Helical and bamboo-shaped CNFs with diameters ranging from 100-200 nm were synthesized.	[67]
KCl, NaCl, K ₂ SO ₄ , Na ₂ SO ₄ , K ₂ CO ₃ , and Na ₂ CO ₃ / - / -	Dip coating	Ethanol / CVD at 820°C for 60 min via aerosol method	Onion-like tips SWCNTs with diameters ranging from 8-23 nm were synthesized.	[68]
NaCl, NaHCO ₃ , Na ₂ CO ₃ , and NaOH / - / Alumina, Silica, Carbon fibres		Acetylene and carbon dioxide / CVD at 390-820°C for 15 min	<ul style="list-style-type: none"> Carbon yield: 95 tubes/μm Short SWCNTs with diameters ranging from 20-40 nm and I_D/I_G at 2.54 were synthesized. 	[69]
Activated carbon supported KOH / KOH / Powdered activated carbon	Impregnation	Acetylene and carbon dioxide / CVD at 480°C for 40 min	<ul style="list-style-type: none"> Carbon yield: 0.34 wt.% MWCNTs with diameters ranging from 43-108 nm were synthesized. 	[71]
Activated carbon supported NaCl / NaCl / Activated carbon		Acetylene and carbon dioxide / CVD at 600°C for 60 min	<ul style="list-style-type: none"> Carbon yield: 31.87 wt.% Curved MWCNTs with diameters ranging between 40 to 80 nm were synthesized. 	[72]

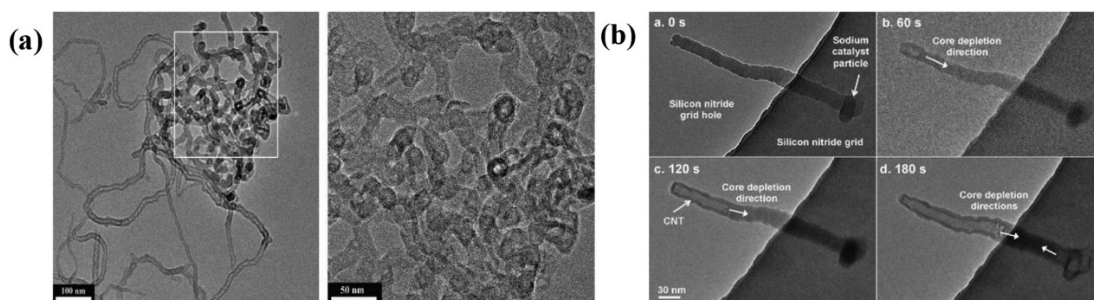


Figure 2.5 Schematic illustrations of CNTs generated from alkali metal catalysts. (a) High tortuosity structure of CNTs produced by NaCl and Na₂CO₃ catalysts [68]. (b) The mechanisms of CNTs formation via NaCl catalysts on Si₃N₄ support [69]. (References permission: Appendix E)

2.2.2 Ni-Based Catalysts

Table 2.2 summarizes the synthesis methods and performances of various types of Ni catalysts, including organo-Ni, Ni monometallic, and Ni bimetallic catalysts, for the growth of CNTs. Ni is considered a promising catalyst for high-yield CNTs growth due to its mild metal-carbon interactions, which strike a balance between the adsorption of carbon sources and the exsolution of carbons necessary for CNTs growth. The presence of a moderate number of vacancies (typically observed in the range of 2 to 4) within the d orbital of Ni catalysts theoretically allows for the formation of metastable Ni carbide, facilitating the nucleation of CNTs [73]. When comparing Ni and Cu catalysts, Ni catalysts tend to produce graphitized bamboo-shaped CNTs, while Cu catalysts yield amorphous carbon and carbon nanocages. This difference in the morphologies of carbon products arises from variations in the vacancies within the d orbitals of Ni and Cu catalysts. Cu catalysts, with fully occupied d orbitals, are unable to react with carbon to form Cu carbides, thus hindering CNTs production [74]. Despite the carbide formation model proposed for Ni catalysts, they are typically associated with the surface diffusion model in initiating CNTs nucleation [54,75,76].